CFD ANALYSIS OF COMPUTATIONAL WIND ENGINEERING APPLICATIONS USING THE FINITE ELEMENT METHOD AND LARGE EDDY SIMULATION

Alexandre Luis Braun, allbraun@ig.com.br
Armando Miguel Awruch, awruch@adufrgs.ufrgs.br
Programa de Pós-Graduação em Engenharia Civil (PPGEC)
Universidade Federal do Rio Grande do Sul (UFRGS)
Av. Osvaldo Aranha, 99 – 3° andar, Porto Alegre, RS, Brasil, CEP 90035-190

Abstract. *The wind action on realistic structures is investigated in this work using numerical tools from Computational Fluid Dynamics (CFD). In recent years, wind tunnel experiments have been carried out by numerical simulation, leading to a new research field on CFD: the Computational Wind Engineering (CWE). A wide variety of problems is now investigated in the field of CWE, including evaluations of aerodynamic coefficients for estimation of the wind action on structures, determination of air flow patterns around and within buildings and simulation of pollutant dispersion in urban areas. In this paper, the flow governing equations are the Navier-Stokes equations and the continuity equation, considering the pseudo-compressibility hypothesis for incompressible flows. The numerical model is obtained using an explicit two-step Taylor Galerkin scheme for the discretization of the flow governing equations in the time domain and the Finite Element Method (FEM) for spatial approximations, which are performed using eight-node hexahedral elements with one-point quadrature. Turbulence flows are analyzed employing Large Eddy Simulation with the dynamic model for sub-grid scales. Some practical examples are simulated in order to validate the numerical model, including the wind action on a bridge, the airflow patterns around a block of buildings in an urban area and the wind circulation around and within a simple building with an opening in the windward wall.*

Keywords*: Computational Wind Engineering (CWE), Computational Fluid Dynamics (CFD), Finite Element Method (FEM), Large Eddy Simulation (LES).*

1. INTRODUCTION

Computational Wind Engineering (CWE) (see Murakami, 1997 and Stathopoulos, 1997 for further details) deals with numerical simulation of classical wind tunnel experiments for evaluations of aerodynamic/aeroelastic effects induced by the wind action on civil structures, such as long-span bridges and buildings. Experimental techniques may be replaced now by reliable algorithms that simulate wind flows with high level of accuracy. In addition, the numerical approach is more attractive than wind tunnel studies because it is much less expensive in terms of time and financial costs. However, wind flows are very difficult to reproduce numerically owing to complex characteristics of the flow field.

The wind action over general structures may be evaluated using aerodynamic or aeroelastic analysis, depending on the level of interaction considered between the fluid and structural fields. Aerodynamic analysis is recommended for determination of wind loads on immersed bodies that are very rigid, such that the elastic effects of the structure on the surrounding flow can be disregarded without losses in the physical representation of the problem. On the other hand, aeroelastic analyses are generally used for identification of dynamic instabilities induced by the wind action over flexible structures. In this work, the aerodynamic approach is employed in all simulations.

The aerodynamic analysis is performed numerically using numerical models to solve the Navier-Stokes equations over the flow field, considering the immersed body as a rigid structure with non-slip boundary conditions. It is well known that the flow field around a 3D bluff body is extremely complicated, since impingement, separation, reattachment, circulation and vortex shedding may occur simultaneously. Moreover, the mathematical treatment of incompressible flows is subjected to restrictions imposed to the continuity equation by the incompressibility assumption (divergence-free condition on the velocity field). Although direct simulation will be possible in a near future for all Reynolds numbers, turbulence modeling is still required in order to represent the effects of small scales over the main flow. Hence, it is observed that almost all those phenomena which are considered hard to solve in the field of Computational Fluid Dynamics (CFD) are included here.

In the present paper, the flow governing equations are the Navier-Stokes equations and a special form of the mass conservation equation, which is obtained using the pseudo-compressibility hypothesis presented by Chorin (1967), leading to an explicit treatment for the pressure field. Turbulent flows are analyzed using Large Eddy Simulation (LES) with the dynamic model for sub-grid scales (see Smagorinsky, 1963 and Lilly, 1992). The numerical scheme for the flow analysis is obtained applying the explicit two-step Taylor-Galerkin method (see Kawahara and Hirano, 1983) to the governing equations set. The Finite Element Method (FEM) is employed for spatial discretizations using the eight-node hexahedrical isoparametric element with one-point quadrature. Typical applications are carried out in order to demonstrate the applicability of the present formulation.

2. THE GOVERNING EQUATIONS FOR WIND FLOWS

Wind flows are usually characterized by the following properties:
1) Natural wind streams are considered to be within the incompressible flow range;
2) Wind is always flowing with a constant temperature (isothermal process);
3) Gravity forces are neglected in the fluid equilibrium;
4) Air is considered as a Newtonian fluid.

Considering the properties presented above and in the absence of structural motion (aerodynamic analysis), the flow governing equation are defined in a classical Eulerian kinematical description by the following expressions (see, for instance, Schlichting, 1979):

a) Momentum conserving equations – the Navier-Stokes equations:

$$\frac{\partial v_i}{\partial t} + v_j \frac{\partial v_i}{\partial x_j} = -\frac{1}{\rho}\frac{\partial p}{\partial x_j} + \frac{1}{\rho}\frac{\partial \sigma_{ij}}{\partial x_j} \qquad (i, j = 1,2,3) \quad \text{in } \Omega^f \tag{1}$$

b) Mass conserving equation for pseudo-compressible flows (see Braun and Awruch, 2005 for further information) – the continuity equation:

$$\frac{\partial p}{\partial t} + v_j \frac{\partial p}{\partial x_j} + \rho c^2 \frac{\partial v_j}{\partial x_j} = 0 \qquad (j = 1,2,3) \quad \text{in } \Omega^f \tag{2}$$

c) Constitutive equation for Newtonian fluids:

$$\sigma_{ij} = -p\delta_{ij} + \tau_{ij} \quad ; \quad \tau_{ij} = \mu\left(\frac{\partial v_i}{\partial x_j} + \frac{\partial v_j}{\partial x_i}\right) + \lambda \frac{\partial v_k}{\partial x_k}\delta_{ij} \qquad (i, j, k = 1,2,3) \tag{3}$$

where v_i are components of the velocity vector in the i direction, x_j are components of the cartesian coordinates vector in the j direction, t indicates the time domain, p is the thermodynamic pressure, ρ is the fluid's specific mass, c is the sound speed in the fluid field and Ω^f is the flow's spatial domain, which is bounded by Γ^{Tf}, δ_{ij} are components of the Kroenecker's delta ($\delta_{ij} = 1$ for $i = j$; $\delta_{ij} = 0$ for $i \neq j$) and μ and λ are the dynamic and volumetric viscosities of the fluid, respectively.

Neumann and Dirichlet boundary conditions must be specified on Γ^{Tf} to solve the flow problem, which are given by the following expressions:

$$v_i = \overline{v}_i \qquad (i = 1,2,3) \quad \text{on } \Gamma^v \tag{4}$$

$$p = \overline{p} \qquad \text{on} \quad \Gamma^p \tag{5}$$

$$\left[-\frac{p}{\rho}\delta_{ij} + \frac{\mu}{\rho}\left(\frac{\partial v_i}{\partial x_j} + \frac{\partial v_j}{\partial x_i}\right) + \frac{\lambda}{\rho}\frac{\partial v_k}{\partial x_k}\right] n_j = \frac{\sigma_{ij} n_j}{\rho} = \overline{S}_i \qquad (i, j, k = 1,2,3) \quad \text{on } \Gamma^\sigma \tag{6}$$

where Γ^v (boundary with prescribed values $\overline{v}_i$ for the fluid velocity field), Γ^p (boundary with prescribed values $\overline{p}$ for the pressure field) and Γ^σ (boundary with prescribed values $\overline{S}_i$ for the fluid boundary tractions) are complementary subsets of the boundary Γ^{Tf}, such that $\Gamma^{Tf} = \Gamma^v + \Gamma^p + \Gamma^\sigma$. In Eq. (7) n_j are components of the unit normal vector **n** at the boundary Γ^σ. Initial conditions for the pressure and velocity fields must be also specified at $t = 0$ to start up the flow analysis.

2.1. The turbulence modeling

Although any viscous incompressible flow can be analyzed with the set of governing equations given above, it is observed that only flows with moderate Reynolds numbers can be in fact simulated using direct simulation, considering the computational capacity of the modern computers. Turbulent flows are very restrictive because the smaller turbulence scales, which are associated to the smaller eddies of the flow field, require computational meshes with very fine definition in order to describe the motion of this flow structures correctly. The turbulence problem is usually solved employing modified governing equations that reproduce the turbulence effects over the main flow statistically. These turbulence effects are represented by means of turbulence models. In this work, LES is used in the turbulence modeling.

In the LES formulation the governing equations are submitted to a spatial filtering process where the flow field is decomposed into large and small scales (or large and small eddies). Large eddies are solved directly with the filtered equations, which are described by field variables associated to the large scales, and eddies smaller than the grid resolution are modeled using turbulence closure models, which are employed in order to represent the small scales effects over the large ones.

The governing equations may be written after the filtering process as follows:

$$\frac{\partial \overline{v}_i}{\partial t} + \overline{v}_j \frac{\partial \overline{v}_i}{\partial x_j} = -\frac{1}{\rho}\frac{\partial \overline{p}}{\partial x_j} + \frac{1}{\rho}\left(\frac{\partial \overline{\sigma}_{ij}}{\partial x_j} + \tau_{ij}^{SGS}\right) \qquad (i, j = 1,2,3) \quad \text{in } \Omega^f \tag{7}$$

$$\frac{\partial \overline{p}}{\partial t} + \overline{v}_j \frac{\partial \overline{p}}{\partial x_j} + \rho c^2 \frac{\partial \overline{v}_j}{\partial x_j} = 0 \qquad (j = 1,2,3) \quad \text{in } \Omega^f \tag{8}$$

where τ_{ij}^{SGS} are components of the Reynolds sub-grid stress tensor (which is associated to unsolved sub-grid terms that must be modeled) and overbars indicate large scale variables. The Reynolds sub-grid tensor is usually approximated according to the Boussinesq assumption:

$$\tau_{ij}^{SGS} = \rho\left(\overline{v_i' v_j'}\right) = 2\mu_t \overline{S}_{ij} \tag{9}$$

where commas indicate sub-grid scale variables, μ_t is the eddy viscosity and $\overline{S}_{ij}$ are components of the strain rate tensor, which are expressed in terms of large scale variables as follows:

$$\overline{S}_{ij} = \frac{1}{2}\left(\frac{\partial \overline{v}_i}{\partial x_j} + \frac{\partial \overline{v}_j}{\partial x_i}\right) \tag{10}$$

The eddy viscosity μ_t must be obtained using some sub-grid scale model. In the present work, this is made employing the dynamic sub-grid scale model. The dynamic model was presented first by Germano et al. (1991) and adjusted later by Lilly (1992).

The eddy viscosity μ_t is usually expressed in the dynamic model as shown below:

$$\mu_t = \rho C(\vec{x},t)\overline{\Delta}^2 \left|\overline{S}\right| \tag{11}$$

where $C(\vec{x},t)$ is the dynamic coefficient (with $\vec{x}$ and t indicating space and time dependencies), $\left|\overline{S}\right|$ is the filtered strain rate tensor modulus and $\overline{\Delta}$ is the characteristic dimension of the grid filter, which is associated to element volumes in FEM formulations ($\overline{\Delta}^{ele} = \sqrt[3]{vol^{ele}}$). The dynamic coefficient is updated along the time integration process taking into account the instantaneous condition of the flow field. The expression due to Lilly (1992) is employed here as follows:

$$C(\vec{x},t) = -\frac{1}{2}\frac{\mathscr{L}_{ij}\mathscr{M}_{ij}}{\mathscr{M}_{ij}\mathscr{M}_{ij}} \tag{12}$$

where:

$$\mathscr{L}_{ij} = \left\langle \overline{v}_i \overline{v}_j \right\rangle - \left\langle \overline{v}_i \right\rangle \left\langle \overline{v}_j \right\rangle \tag{13}$$

and:

$$\mathscr{M}_{ij} = \left\langle \overline{\Delta}^2 \right\rangle \left|\left\langle \overline{S} \right\rangle\right| \left\langle \overline{S}_{ij} \right\rangle - \left\langle \Delta^2 \left|\overline{S}\right| \overline{S}_{ij} \right\rangle \tag{14}$$

The solution of Eq. (12) demands two filtering processes on the flow governing equations: the first filtering is associated to the use of the LES formulation, which is related to grid filter $\overline{\Delta}$ and large scale variables represented by overbars ($\overline{\bullet}$). The second filtering is referred to a second filter called test filter $\left\langle \overline{\Delta} \right\rangle$, which must be larger than the first filter $\overline{\Delta}$. Second filtering variables are identified by the symbol $\langle \bullet \rangle$ and they are computed using the expression below:

$$\left\langle \overline{k} \right\rangle^i = \frac{\sum_{j=1}^{n}\left(\frac{\overline{k}^j}{d_i^j}\right)}{\sum_{j=1}^{n}\left(\frac{1}{d_i^j}\right)} \tag{15}$$

where $\left\langle \overline{k} \right\rangle^i$ is the second filtering value at the nodal point *i* of a generic variable $\overline{k}$, which is associated to large scales of the first filtering, *n* is the number of nodal points with direct connectivity to the nodal point *i*, d_i^j is the distance between the nodal points *i* and *j* and $\overline{k}^j$ is the first filtering value of a generic variable *k* computed at the nodal point *j*. The second filter arrangement is illustrated in Fig. 1.

The characteristic dimension of the second filter at a nodal point *i* is determined by:

$$\left\langle \overline{\Delta} \right\rangle^i = \sqrt[3]{\sum_{p=1}^{ne} vol(p)} \tag{16}$$

where *ne* is the number of elements in the neighborhood of node *i* and *vol*(p) is the volume of the element p.

The final form of the governing equations with turbulent effects is written as follows:

$$\frac{\partial \overline{v}_i}{\partial t} + \overline{v}_j \frac{\partial \overline{v}_i}{\partial x_j} = -\frac{1}{\rho}\frac{\partial \overline{p}}{\partial x_j} + \frac{1}{\rho}\frac{\partial}{\partial x_j}\left[\left(\mu + \mu_t\right)\left(\frac{\partial \overline{v}_i}{\partial x_j} + \frac{\partial \overline{v}_j}{\partial x_i}\right) + \lambda \frac{\partial \overline{v}_k}{\partial x_k}\delta_{ij}\right] \qquad (i,j,k = 1,2,3) \quad \text{in } \Omega^f \tag{17}$$

$$\frac{\partial \overline{p}}{\partial t} + \overline{v}_j \frac{\partial \overline{p}}{\partial x_j} + \rho c^2 \frac{\partial \overline{v}_j}{\partial x_j} = 0 \qquad (j = 1,2,3) \quad \text{in } \Omega^f \tag{18}$$

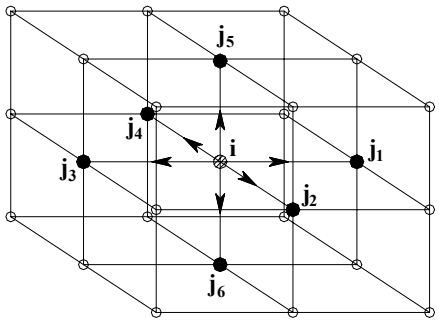

Figure 1. Second filter arrangement.

3. THE NUMERICAL MODEL FOR THE FLOW ANALYSIS

The explicit two-step Taylor-Galerkin scheme is employed in this work for the time discretization of the flow governing equations. Additional information about this numerical model may be found in Kawahara and Hirano (1983) and Braun and Awruch (2003). The algorithm for the flow simulation may be summarized in the following steps:

(1) Calculate $v_i^{n+1/2}$ with:

$$v_i^{n+1/2} = v_i^n + \frac{\Delta t}{2}\left\{-v_j \frac{\partial v_i}{\partial x_j} - \frac{1}{\rho}\frac{\partial p}{\partial x_j}\delta_{ij} + \frac{\partial}{\partial x_j}\left[\frac{\mu + \mu_t}{\rho}\left(\frac{\partial v_i}{\partial x_j} + \frac{\partial v_j}{\partial x_i}\right) + \frac{\lambda}{\rho}\frac{\partial v_k}{\partial x_k}\delta_{ij}\right] + \left(\frac{\Delta t}{4} v_j v_k\right)\frac{\partial^2 v_j}{\partial x_j x_k}\right\}^n \tag{19}$$

(2) Imposition of the boundary conditions (4) and (6) on $v_i^{n+1/2}$.

(3) Calculate $p^{n+1/2}$ with:

$$p^{n+1/2} = p^n + \frac{\Delta t}{2}\left\{\left[-v_j \frac{\partial p}{\partial x_j} - \rho c^2 \frac{\partial v_j}{\partial x_j}\right] + \left(\frac{\Delta t}{4} v_i v_j\right)\frac{\partial^2 p}{\partial x_j \partial x_i}\right\}^n \tag{20}$$

(4) Imposition of the boundary condition (6) on $p^{n+1/2}$.

(5) Calculate the incremental pressure field with:

$$\Delta p^{n+1/2} = p^{n+1/2} - p^n \tag{21}$$

(6) Calculate $v_i^{n+1/2}$ with:

$$v_i^{n+1/2} = v_i^{n+1/2} - \frac{1}{\rho}\frac{\Delta t^2}{8}\frac{\partial \Delta p^{n+1/2}}{\partial x_i} \tag{22}$$

(7) Imposition of the boundary conditions (4) and (6) on $v_i^{n+1/2}$.

(8) Update velocity field with $v_i^{n+1} = v_i^n + \Delta v_i^{n+1/2}$, where:

$$\Delta v_i^{n+1/2} = \Delta t\left\{-v_j \frac{\partial v_i}{\partial x_j} - \frac{1}{\rho}\frac{\partial p}{\partial x_j}\delta_{ij} + \frac{\partial}{\partial x_j}\left[\frac{\mu + \mu_t}{\rho}\left(\frac{\partial v_i}{\partial x_j} + \frac{\partial v_j}{\partial x_i}\right) + \frac{\lambda}{\rho}\frac{\partial v_k}{\partial x_k}\delta_{ij}\right]\right\}^{n+1/2} \tag{23}$$

(9) Imposition of the boundary conditions (4) and (6) on v_i^{n+1}.

(10) Update pressure field with $p^{n+1} = p^n + \Delta p^{n+1/2}$, where:

$$\Delta p^{n+1/2} = \Delta t\left\{-v_j \frac{\partial p}{\partial x_j} - \rho c^2\left(\frac{\partial v_j}{\partial x_j}\right)\right\}^{n+1/2} \tag{24}$$

(11) Imposition of the boundary condition (6) on p^{n+1}.

The final form of the numerical model is obtained applying the Bubnov-Galerkin's weighted residual scheme into the FEM context on the discrete forms of the flow governing equations. Eight-node hexahedral elements are used for spatial approximations employing the one-point quadrature technique for the evaluation of element matrices. An efficient method for hourglass control in the fluid mesh is adopted according to the model proposed by Christon (1997). Further information about FEM applications on fluid dynamics may be found in Reddy and Gartling (1994) and Zienkiewicz et al. (2005).

4. THE NUMERICAL EVALUATION OF AERODYNAMIC COEFFICIENTS

The use of aerodynamic coefficients is very popular in Wind Engineering analyses and many analytical models to describe aerodynamic/aeroelastic phenomena are formulated using this important information. Aerodynamic forces are developed over the body surface of structures immersed in a fluid stream. These forces are usually obtained by the integration of pressures and shear stresses developed on the fluid-structure interface owing to the flow action. The components of the aerodynamic forces in the along-flow and across-flow directions are referred to as drag and lift, respectively.

The aerodynamic coefficients are evaluated in this work using the formulae below:

$$C_{Fx} = \frac{\sum_{i=1}^{NNI}\left(F_x\right)^i}{1/2\,\rho V_\infty^2 HW};\quad C_{Fy} = \frac{\sum_{i=1}^{NNI}\left(F_y\right)^i}{1/2\,\rho V_\infty^2 HL};\quad C_{Fz} = \frac{\sum_{i=1}^{NNI}\left(F_z\right)^i}{1/2\,\rho V_\infty^2 WL}$$
$$C_{Mz} = \frac{\sum_{i=1}^{NNI}\left(F_y\Delta_x - F_x\Delta_y\right)^i}{1/2\,\rho V_\infty^2 HLW};\quad C_{Mx} = \frac{\sum_{i=1}^{NNI}\left(F_z\Delta_y - F_y\Delta_z\right)^i}{1/2\,\rho V_\infty^2 H^2 L};\quad C_{My} = \frac{\sum_{i=1}^{NNI}\left(F_x\Delta_z - F_z\Delta_x\right)^i}{1/2\,\rho V_\infty^2 H^2 W} \tag{25}$$

with:

$$\left(\Delta_x\right)^i = X_i - X_g$$
$$\left(\Delta_y\right)^i = Y_i - Y_g \tag{26}$$
$$\left(\Delta_z\right)^i = Z_i - Z_g$$

where X_i, Y_i and Z_i are Cartesian global coordinates of a nodal point *i* on the fluid-structure interface, X_g, Y_g and Z_g are Cartesian global coordinates of the body gravity center, V_∞ is the flow reference speed, NNI is the number of fluid nodal points on the body surface and L, W and H are characteristic dimensions related to length, width and height of the immersed body. The aerodynamic forces F_x, F_y and F_z at a nodal point *i* are obtained by numerical integration of Eq. (6) over the body surface as follows:

$$\left(F_x\right)^i = -\left(t_1\right)^i\left(A_S\right)^i = -\left[\left(\tau_{1j}\right)^i - \left(p\right)^i\delta_{1j}\right]\left(n_j\right)^i\left(A_S\right)^i$$
$$\left(F_y\right)^i = -\left(t_2\right)^i\left(A_S\right)^i = -\left[\left(\tau_{2j}\right)^i - \left(p\right)^i\delta_{2j}\right]\left(n_j\right)^i\left(A_S\right)^i \tag{27}$$
$$\left(F_z\right)^i = -\left(t_3\right)^i\left(A_S\right)^i = -\left[\left(\tau_{3j}\right)^i - \left(p\right)^i\delta_{3j}\right]\left(n_j\right)^i\left(A_S\right)^i$$

where $\left(A_S\right)^i$ is the influence area of a nodal point *i* at the fluid-structure interface, which may be obtained by some smoothing procedure taking into account face areas of elements in the neighborhood of the node *i*, and $\left(n_j\right)^i$ are components of the unit normal vector **n** at the same nodal point *i*. Although nodal values for the pressure field $\left(p\right)^i$ are obtained by the flow analysis straightforwardly, viscous stresses are variables given at element level in FEM formulations and thus, they must be evaluated at nodal level using smoothing techniques. In this paper the viscous stresses at a nodal point *i* on the body surface are calculated in the following manner:

$$\tau_{ij}^A = \frac{\sum_{k=1}^{NFC}\left(\tau_{ij}\right)_k\,\Gamma_k}{\sum_{k=1}^{NFC}\Gamma_k} \tag{28}$$

where NFC is the number of elements in the neighborhood of a nodal point A at the fluid-structure interface, Γ_k is the face area of the element *k* and $\left(\tau_{ij}\right)_k$ are shear stress components of the element *k*, which are evaluated at the finite element center according to the reduced integration technique.

5. NUMERICAL APPLICATIONS

5.1 Aerodynamic analysis of a bridge cross-section

This first numerical application presents the aerodynamic analysis of a bridge cross-section. The bridge is submitted to different wind incidences in order to obtain circulation patterns of the wind flow around the bridge deck and the aerodynamic coefficients as functions of the angle of attack of the incident wind stream. Figure 2 shows the geometrical

characteristic of the computational domain, which is constituted by 473000 elements. It is observed that the boundary conditions on the external boundaries are given as functions of the angle of attack (α) to reproduce inflow conditions with oblique incidence. Physical properties of the wind flow as well as geometrical and numerical constants used in the numerical simulations are presented in Tab. 1. All simulations are carried out with a Reynolds number Re = $9x10^4$ (Re = $\rho V_0 D/\mu$).

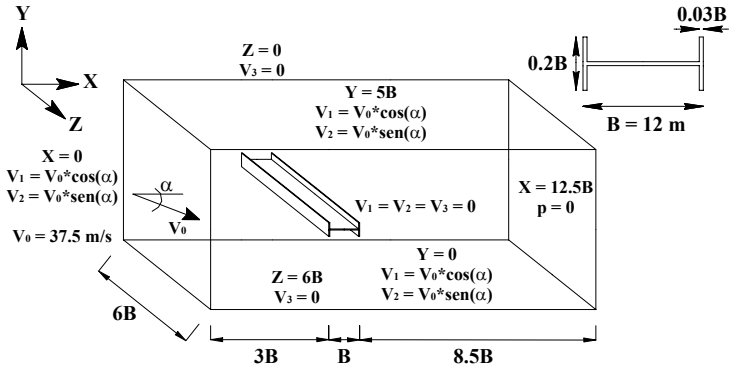

Figure 2. Geometrical characteristics of the computational domain used in the bridge analysis.

Table 1. Constants employed in the aerodynamic analysis of a bridge.

Specific mass (ρ)	1.25 Kg/m^3
Dinamic viscosity (μ)	$1.25x10^{-3}$ Ns/m^2
Volumetric viscosity (λ)	0.0 Ns/m^2
Sound speed (c)	150.0 m/s
Reference velocity – V_0	37.5 m/s
Characteristic dimension – D (= 0.2B)	2.4 m
Time step (Δt)	$1x10^{-4}$ s

Table 2 presents time-average values obtained by the present work in the aerodynamic analysis of the bridge cross-section proposed above. These values were calculated from time histories that are referred to drag, lift and moment resultants collected along the numerical simulation. Results referred to the experimental work performed by Limas (2003) in wind tunnel studies are also presented, where a good agreement can be observed between numerical and experimental data. The aerodynamic coefficients C_D, C_L and C_M are given as follows:

$$C_D(\alpha) = C_x(\alpha)\cos(\alpha) + C_y(\alpha)\mathrm{sen}(\alpha)$$
$$C_L(\alpha) = C_y(\alpha)\cos(\alpha) - C_x(\alpha)\mathrm{sen}(\alpha) \quad (29)$$

and:

$$C_x = \frac{\sum F_x}{1/2\,\rho V_0^2 D} \quad ; \quad C_y = \frac{\sum F_y}{1/2\,\rho V_0^2 D} \quad ; \quad C_M = \frac{\sum M_z}{1/2\,\rho V_0^2 D^2} \quad (30)$$

where M_z is the aerodynamic moment acting around an axis passing through the geometrical center of the cross-section and normal to the plane x_1-x_2.

Table 2. Aerodynamic coefficients obtained in the bridge analysis.

References	**Angle of wind incidence**	**Aerodynamic coefficients**		
		C_D	**C_L**	**C_M**
Present work	-8°	0.52	-0.79	0.05
	-4°	0.32	-0.25	0.02
	0°	0.28	0.0	0.0
	+4°	0.31	0.28	-0.02
	+8°	0.51	0.80	-0.04
Limas (2003)	-8°	0.44	-0.66	0.05
	-4°	0.33	-0.38	0.02
	0°	0.28	-0.04	0.01
	+4°	0.34	0.44	-0.04
	+8°	0.49	0.79	-0.04

The flow circulation around the bridge can be analyzed in Fig. 3, where pressure fields and streamlines obtained in the numerical simulation for different wind incidences are presented. It is important to notice that figures are related to instantaneous fields of the pre-referred variables. Important conclusions can be made in terms of aerodynamic behavior of the bridge studied in this paper comparing results presented in Tab. 2 and the flow conditions observed in Fig. 3. It is verified that the minimum lift value at $\alpha = 0°$ is related to similar pressure fields developed above and below the bridge deck. On the other hand, at $\alpha = -8°$ and $\alpha = +8°$ maximum lift values are obtained because force resultants due to pressure distribution on the bridge surface are clearly developed in the x_2 direction with the lift sign given according to the angle of wind incidence. Drag force is minimum at $\alpha = 0°$ owing to the fact that the frontal wall is the unique area of the bridge cross-section with direct exposure to the wind stream. Aerodynamic moments are always observed for nonzero incidence angles due to unbalanced pressure distributions generated on the bridge by the wind action.

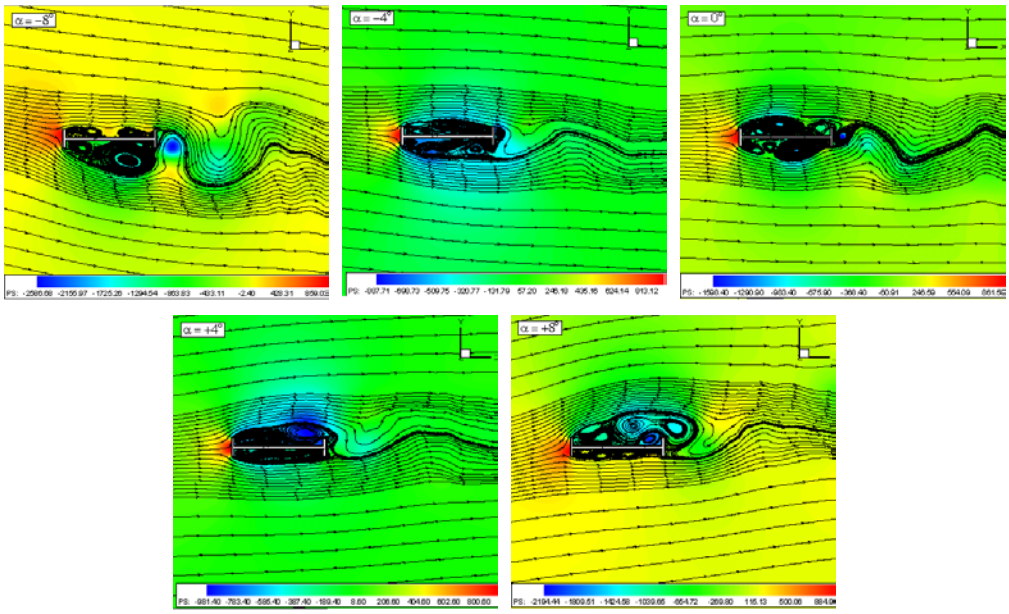

Figure 3. Instantaneous pressure fields and streamlines for the bridge analysis.

5.2 Wind environment conditions around a block of buildings

In the present application a typical urban area is selected as a test case for the computation of wind environment conditions around buildings immersed in a flow with atmospheric boundary layer characteristics. Information about geometrical properties and boundary conditions of the computational domain as well as locations of points of measurements of wind speeds are presented in detail in Fig. 4.

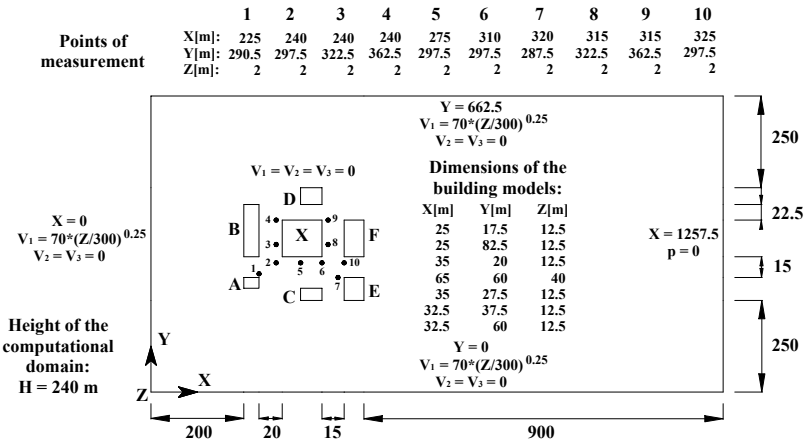

Figure 4. Geometrical characteristics of the computational domain referred to the block of buildings.

The computational grid is constituted by 1268272 elements. Fluid properties are presented in Tab. 3 with additional constants employed in the numerical analysis. The present simulation is performed with a Reynolds number $Re = 10^5$ ($Re = \rho V_0 D/\mu$).

Table 3. Constants employed in the wind environment analysis of a block of buildings.

Specific mass (ρ)	1.25 Kg/m^3
Dinamic viscosity (μ)	3.17x10^{-2} Ns/m^2
Volumetric viscosity (λ)	0.0 Ns/m^2
Sound speed (c)	230.0 m/s
Reference velocity – V_0	42.3 m/s
Characteristic dimension – D (= 0.2B)	60 m
Time step (Δt)	6x10^{-4} s

Time-average pressure fields computed by the present work are shown in Fig. 5. It is verified that zones with high pressure are developed in the frontal area of the block of buildings for Z = 5 m and Z = 10 m owing to the action of horseshoe vortices (see Peterka et al., 1985 for further details) near the ground. Zones with complex flow characteristics are also observed between the buildings A and X for Z = 5 m and Z = 10 m, where a recirculating region with high suction is generated. It is observed that the building X is submitted to larger pressure zones on the frontal surface as well as larger separation areas on the lateral walls due to direct incidence of the wind stream for Z = 25 m and Z = 40 m.

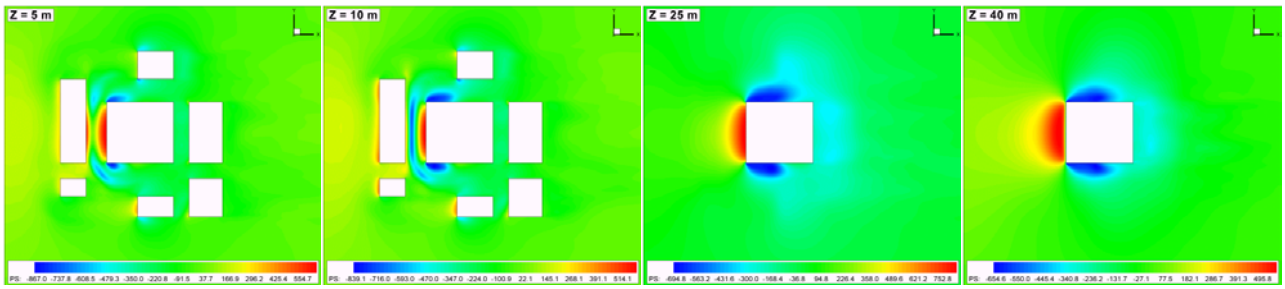

Figure 5. Time-average pressure fields referred to the wind environment analysis of a block of buildings.

The time-average wind speed W ($W = \sqrt{v_1^2 + v_2^2} / V_{in}$; V_{in} = inflow wind speed at Z = 2 m) obtained by the present work at some points of measurement indicated in Fig. 4 are shown in Tab. 4. The present results are compared to experimental and numerical data obtained by Stathopoulos and Baskaran (1996), where a reasonable agreement can be observed.

Table 4. Time-average wind speed W at points of measurements.

Point of measurement	**Time-average wind speed W**		
	Present work	**Stathopoulos and Baskaran (1996)**	
		Numerical	**Experimental**
1	0.80	0.73	0.98
2	1.49	0.98	1.32
3	0.34	0.57	0.23
4	1.43	1.08	1.28
5	1.26	0.89	1.02
6	1.14	0.81	0.67
7	0.60	0.96	0.76
8	0.27	0.26	0.05
9	0.61	0.58	0.44
10	0.83	0.84	0.64

5.3 Ventilation analysis of a building model with an opening

The present application deals with the computation of airflow conditions around and within a building-like body with an opening in windward wall, which is immersed in a wind flow with atmospheric boundary layer characteristics. A schematic view of the computational domain with the respective boundary conditions and points of velocity measurements may be found in Fig. 6. The computational grid is constituted by 1037660 elements. Fluid properties are presented in Tab. 5 with additional constants employed by the numerical algorithm. The present simulation is

performed with a Reynolds number Re = $1.4x10^5$, which is calculated using the inflow velocity at Z = 2.5 m (V_{ref}) and the building height H = 2.5 m.

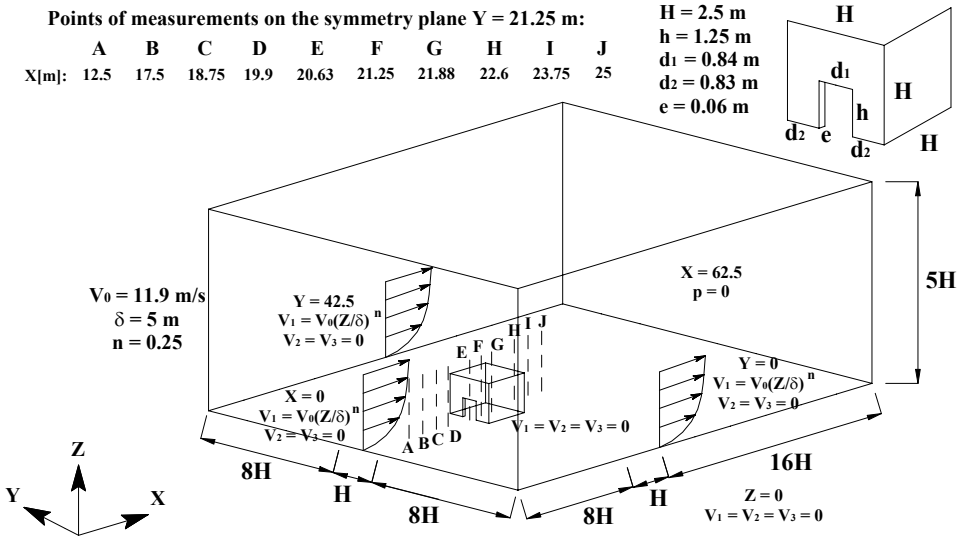

Figure 6. Schematic view of the computational domain for the ventilation analysis.

Table 5. Constants employed in the ventilation analysis of a building-like model.

Specific mass (ρ)	1.25 Kg/m^3
Dinamic viscosity (μ)	$3.17x10^{-2}$ Ns/m^2
Volumetric viscosity (λ)	0.0 Ns/m^2
Sound speed (*c*)	230.0 m/s
Reference velocity – V_0	42.3 m/s
Characteristic dimension – D (= 0.2B)	60 m
Time step (Δt)	$6x10^{-4}$ s

Figure 7 shows time-average velocity profiles in the streamwise direction computed by the present work at the points of measurement indicated in Fig. 6. The present results (solid lines) are compared to experimental data (black dots) by Jiang et al. (2003), where a good agreement can be verified. Differences between numerical and experimental data are related to turbulence fluctuations considered in the wind tunnel analysis.

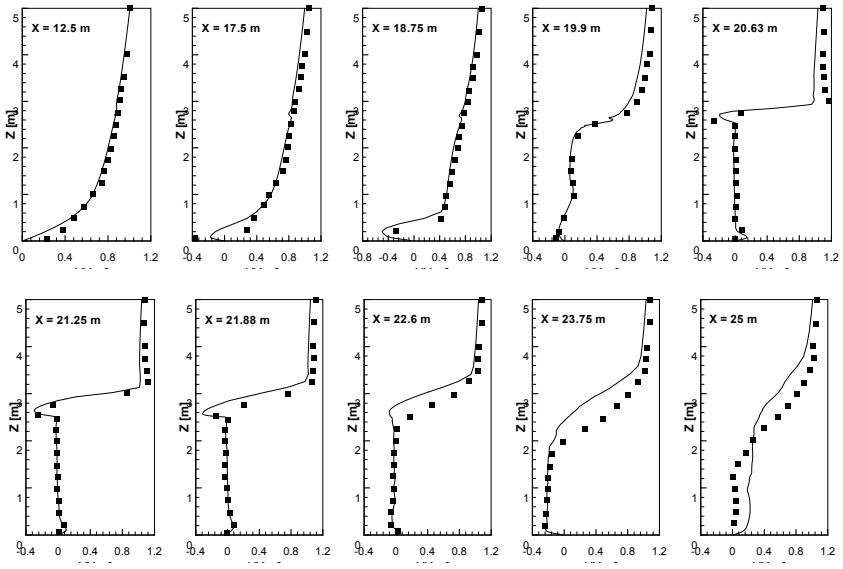

Figure 7. Schematic view of the computational domain for the ventilation analysis.

Instantaneous pressure fields obtained by the present work are shown in Fig. 8. It is observed that high pressure fields are developed inside the building model preventing airflow entering and leading to inactive flow motions. On the other hand, the outer flow is very similar to airflows observed around cubic models without openings.

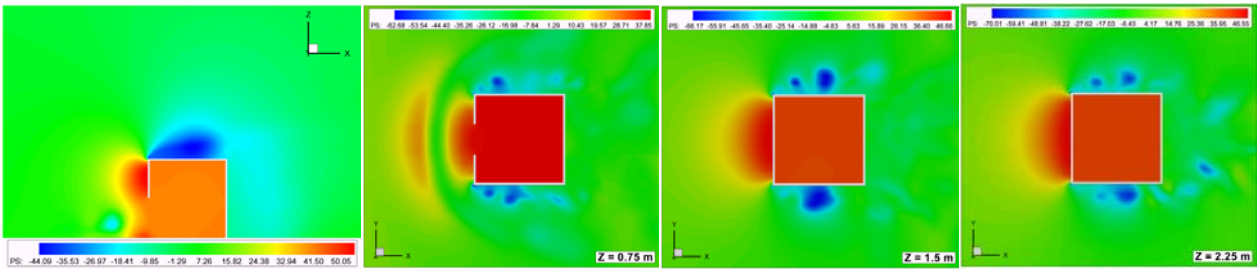

Figure 8. Instantaneous pressure fields obtained in the ventilation analysis.

6. CONCLUSIONS

A numerical model to simulate Wind Engineering problems was presented in this work. Some typical applications were analyzed where results obtained by the present algorithm were compared to experimental data from wind tunnel studies. It was verified that the numerical scheme proposed in this paper predicted well the physical phenomena related to the examples simulated here. Some improvements may be performed in the present formulation in order to obtain a better approach for the physical problem as well as a more efficient code. Suggestions include implementation of a numerical model to consider turbulence fluctuations in the inflow boundary conditions and a numerical algorithm for adaptative meshes.

7. REFERENCES

Braun, A.L. and Awruch, A.M., 2003, "Numerical simulation of the wind action on a long-span bridge deck", Journal of the Brazilian Society of Mechanical Science and Engineering, vol. XXV, n° 4, pp. 352-363.

Braun, A.L. and Awruch, A.M., 2005, "Aerodynamic and aeroelastic analysis of bundled cables by numerical simulation", Journal of Sound and Vibration, vol. 284, pp. 51-73.

Chorin, A.J., 1967, "A numerical method for solving incompressible viscous flow problems", Journal of Computational Physics, vol. 2, pp. 12-26.

Christon, M.A., 1997, "A domain-decomposition message-passing approach to transient viscous incompressible flow using explicit time integration", Computer Methods in Applied Mechanics and Engineering, vol. 148, pp. 329-352.

Germano, M., Piomelli, U., Moin, P. and Cabot, W.H., 1991, "A dynamic subgrid-scale eddy viscosity model", Physics of Fluids, vol. A3, n. 7, pp. 1760-1765.

Jiang, Y., Alexandre, D., Jenkins, H., Arthur, R. and Chen, Q., 2003, "Natural ventilation in buildings: measurements in a wind tunnel and numerical simulation with large-eddy simulation", Journal of Wind Engineering and Industrial Aerodynamics, vol. 91, pp. 331-353.

Kawahara, M. and Hirano, H., 1983, "A finite element method for high Reynolds number viscous fluid flow using two step explicit scheme", International Journal for Numerical Methods in Fluids, vol. 3, pp. 137-163.

Lilly, D.K., 1992, "A proposed modification of the Germano subgrid-scale closure method", Physics of Fluids, vol. A4, n. 3, pp. 633-635.

Limas, L.F., 2003, "Determinação das Características Aerodinâmicas de Seções Transversais de Pontes em Túnel de Vento", Dissertação de Mestrado, PPGEC/UFRGS, Porto Alegre.

Murakami, S., 1997, "Current status and future trends in computational wind engineering", Journal of Wind Engineering and Industrial Aerodynamics, vol. 67&68, pp. 3-34.

Peterka, J.A., Meroney, R.N. and Kothari, K.M., 1985, "Wind flow patterns about buildings", Journal of Wind Engineering and Industrial Aerodynamics, vol. 21, pp. 21-38.

Reddy, J.N. and Gartling, D.K., 1994, "The Finite Element Method in the Heat Transfer and Fluid Dynamics", Boca Raton, Florida: CRC Press.

Schlichting, H., 1979, "Boundary-Layer Theory", New York: McGraw-Hill Inc., 2nd ed.

Smagorinsky, J., 1963, "General circulation experiments with the primitive equations, I, the basic experiment", Monthly Weather Review, vol. 91, pp. 99-135.

Stathopoulos, T., 1997, "Computational wind engineering: Past achievements and future challenges", Journal of Wind Engineering and Industrial Aerodynamics, vol. 67&68, pp. 509-532.

Stathopoulos, T. and Baskaran, A., 1996, "Computer simulation of wind environment conditions around buildings", Engineering Structures, vol. 18, n° 11, pp. 876-885.

Zienckiewicz, O.C., Taylor, R.L. and Nithiarasu, P., 2005, "The Finite Element Method for Fluid Dynamics", Oxford: Elsevier Butterworth-Heinemann, 6th ed.